Phase Shift of the Keplerian Orbits inside Dark Matter Halos

Saoussan Kallel-Jallouli

Faculté des Sciences de Tunis; Department of Mathematics, Université de Tunnis El Manar, LR03ES04, Tunis, 2092, Tunisia

DOI: https://doi.org/10.51244/IJRSI.2024.11110038

Received: 07 October 2024; Accepted: 05 November 2024; Published: 06 December 2024

ABSTRACT

A new theory proposed the existence of a new kind of unseen staff named "Zaman", responsible for the flow of time by its spin. Zaman solves the Dark Matter enigma. Moreover, for an isolated Zaman spherical halo U with differential rotation, if the relation between the radius of each shell R and the length T of its day is Keplerian; that is $\frac{T^2}{R^3}$ is constant, then, we proved the known linear Hubble relation is satisfied. In this work, we shall see how some distances can be elongated. We shall prove the Keplerian trajectories are discontinuous. More precisely, after each period, any test particle inside U will receive an instantaneous kick-off to be shifted from its initial orbital phase.

Keywords: Hubble constant, Kepler, Time, phase-shift, Velocity, Zaman Dark Matter

PACS : 95.35.+d, 98.80.Es, 06.30.Ft, 06.30.Gv, 42.87.Bg

INTRODUCTION

Recently, a new model was suggested to solve the enigma of Dark Matter (DM) [Kallel-Jallouli, 2018, 2021a,b,c,d]. Kallel proved the existence of an unusual unseen staff, called Zaman, responsible for the flow of time by its spin. The proposed model offers a solution for the dark matter puzzle. Kallel firstly studied the simple case of a solid body rotating spherical Zaman [Kallel-Jallouli, 2023, 2024c]. She explained the relation between U-spin and U-time and aging [Kallel-Jallouli, 2024d]. In reality, solid body rotation is a very special case. In most cases, we also have differential rotation, where, for each shell of radius r inside U, the length T(r) of its U-day depends on r [Kallel-Jallouli, 2024a]. In the special case when $\frac{T^2(r)}{r^3}$ is constant, Kallel deduced the Hubble law, without any need for any supplementary hypothesis or any special non Euclidian geometry, as proposed by Lerner et al. [2014] for their observations to be matched with the laws of nature. In this work, we shall prove the discontinuity of the Keplerian orbits. More precisely, after each cycle, any test particle receives a kick-off to be shifted from its previous phase position.

Time and phase relation

For a Zaman sphere U with solid body rotation with respect to a non-rotating state U_I, let us select the isotime-disc enclosed in the plane (Oxz) as the semidisc of U-time 0 (see [Kallel-Jallouli, 2021b, fig. 2] Any point P in U_I with coordinates (r, θ, φ) indicates the space position (r, θ, φ) and the U-time variation inside U. For the first day, we have the relation [Kallel-Jallouli, 2021a,b,c]:

$$t_U = T - \frac{T}{2\pi}\theta = T\left(1 - \frac{\theta}{2\pi}\right) \quad \text{(from } 0 \text{ to } T\text{).} \qquad (1)$$

For the n^{th} day, U-time is given by:

$$t_U = nT - \frac{T}{2\pi}\theta = T\left(n - \frac{\theta}{2\pi}\right) \quad \text{(between } (n\text{-}1)T \text{ and } nT\text{).} \qquad (2)$$

ISSN No. 2321-2705 | DOI: 10.51244/IJRSI |Volume XI Issue XI November 2024

More generally, for a Zaman sphere U with differential rotation, if we suppose time is universal inside U and the U-time $t_U(R)$ does not depend on R, then, for each spherical shell of radius R inside U, the n[th] day, U-time t_U is provided by [Kallel-Jallouli, 2024a]:

$$t_U = nT(R) - \frac{T(R)}{2\pi}\theta = T(R)\left(n - \frac{\theta(R)}{2\pi}\right) \quad \text{(between } (n\text{-}1)T(R) \text{ and } nT(R)\text{)}, \quad (3)$$

with

$$n = Int\left[\frac{t_U}{T(R)} + 1\right] \qquad (4)$$

The relation (3)(4), can also be written as:

$$\frac{\theta(R)}{2\pi} = Int\left[\frac{t_U}{T(R)}\right] + 1 - \frac{t_U}{T(R)} \qquad (5)$$

Special case: Keplerian orbits inside an isolated Zaman DM halo U

We are interested with the special case of the differential rotation, where, we suppose for each shell of radius $R \geq R_0$, the length T(R) of the U-day satisfies the Keplerian relation between the radius R and the period T [Kallel-Jallouli, 2024a]:

$$\frac{T^2}{R^3} = k \qquad (6)$$

With $k = k(U)$ is a fixed constant.

In this case, the test particles move in Keplerian orbits. We can call our system U: an "outer Keplerian universe" (OKU). Evidently, U can be infinitely small (smaller than an atom), or infinitely large (larger than our detectable universe). There is no restriction on the dimensions for U.

Hubble's law

If the relation (6) is satisfied, it was shown that the radial velocity V_r of each test particle, placed at a distance R$\geq R_0$ from the central origin, is given, almost everywhere, by the classical Hubble's law [Kallel-Jallouli, 2024a]:

$$V_r = \frac{dR}{dt_U} = R' = H(t_U).R \qquad (7)$$

The relation (7) is valid for $t_U \epsilon \bigcup_{n>1}\left](n-1)\sqrt{kR^3}, n\sqrt{kR^3}\right[$. The Hubble constant is given by:

$$H(t_U) = \frac{2}{3}(t_U)^{-1} \qquad (8)$$

Which is inversely proportional to the age t_U of the system U.

Examples

Our universe U is a good example of (OKU). The Hubble law (7) describes the relationship between a galaxy's radial velocity and its distance from us. Nevertheless, as Kallel explained [Kallel-Jallouli, 2018], our universe U is not isolated. Therefore, depending on the impact of the container, the measured Hubble constant can vary [Perivolaropoulos, 2014]. Moreover, our universe contains many subhaloes. Each galaxy G lives inside a subhalo U_G. This galaxy G can be a part of a group or a galaxy cluster living inside a bigger halo U_{Cl}. Evidently, each halo U_G, U_{Cl} has its corresponding age t_{U_G}, $t_{U_{Cl}}$. There is no reason for the ages t_{U_G}, $t_{U_{Cl}}$ and

ISSN No. 2321-2705 | DOI: 10.51244/IJRSI |Volume XI Issue XI November 2024

t_U to be equal. But, t_{U_G}, $t_{U_{Cl}}$ must not be greater than the age t_U of our universe. Consequently, there is no reason for the corresponding Hubble constants H_{U_G}, $H_{U_{Cl}}$ to be equal. But, they must not be smaller than our universe Hubble constant H_U. Therefore, it is normal to find different values for the Hubble constant, depending on the selected samples and their host halos [Riess et al. 2011]. The use of 15 Milky Way (MW) Cepheids, results in a value of H_{MW}~76.18 ± 2.37 km s^{-1} Mpc^{-1} for the MW halo [Riess et al. 2016]. The Use of the Large Magellanic Cloud LMC (a satellite galaxy of the Milky Way), results in a value of 72.04 ± 2.67 km s^{-1} Mpc^{-1} [Riess et al. 2016].

Using the approximate value of 74 km s^{-1} Mpc^{-1} for U, we can deduce from (8),

$$t_{MW} = \frac{2}{3}\frac{1}{74} = \frac{3.086 \times 10^{19}}{3 \times 37} \sim 27 \times 10^{16} s$$

Since one year is approximately 31557600 s, then, $t_{MW} \sim 8.5 \times 10^9 yers \sim 8.5$ billion years.

The Milky Way Galaxy, was formed approximately 8.5 billion years ago.

In our model, the Hubble constant H_U is related to the Keplerian (6) relation and the consequent recessing motion (7) (apparent Dark energy effect). It is also related to the age of U (8). H_U is not connected to any potential rate of expansion of the OKU U.

Hubble tension

We saw how the Hubble constant H_U depends on the OKU U. Consequently, if we chose different subhaloes U_S, there is no reason for their Hubble constant H_{U_S} to be equal, if their birth dates are different.

Now, we shall use the idea proposed by Kallel [Kallel-Jallouli, 2018], were our universe was born inside the crust of a huge tectonic iceball, named "Feluc", and is growing from sublimation of the surrounding ice. Light from our universe will be absorbed and reflected by the surrounding spherical icy surface, at radius $a(t)$ from the spherical universe center (observer). Ice sublimation will make the radius $a(t)$ bigger. The scattered light from the receding icy spherical surface (surface of last scattering SLS) will travel freely through the universe, redshifting to microwave frequencies. We observe those primordial photons today as the cosmic microwave background (CMB), filling all space. CMB was discovered in 1964 by Arno Penzias and Robert Wilson [Dicke et al., 1965].

The recession celerity $a'(t)$ of the surface of last scattering (related to ice sublimation) remains imprinted in the CMB (Doppler effect) [Planck Collaboration. 2016]. Our universe growth rate H_{SLS} (related to ice sublimation rate), defined by:

$$H_{\mathrm{SLS}}(t) = \frac{a'(t)}{a(t)} \qquad (9)$$

can be deduced after taking into account the redshift of photons as they climb out of potential wells to reach us. We need then the use of the Hubble constant H_{U} deduced from (7) [Clifton et al. 2012].

The latest estimate of the growth rate H_{SLS} based on CMB observations by the *Planck* satellite is H_{SLS} = 67.4 ± 0.5 km s^{-1} Mpc^{-1} [Planck Collaboration 2020].

We have two completely different constants: (i) The Hubble constant H_{U} (Dark energy manifestation), related to the Kepler's law (6) and the consequent recessing velocities (7). (ii) The growth rate H_{SLS} (ice sublimation manifestation), related to the SLS recession velocity (9).

We cannot speak about "H_0 Tension". To find the Hubble constant H_{U}, we only need to search for the rate of recession of faraway galaxies. However, to find the growth rate H_{SLS}, since CMB traverses through a radius of the universe to reach us, much work is needed. We need first to calculate H_{U}.

ISSN No. 2321-2705 | DOI: 10.51244/IJRSI |Volume XI Issue XI November 2024

Distance elongation

How do we see a disc of radius r placed in the equator, inside U, at a universal time $t_U = t_0$, with the center O' placed at a distance R>r from the central halo origin O? Suppose the elapsed time t_U inside U does not change with R (time is universal).

Since at time t_0 the least distant point P_{min} is at a distance $(R - r)$ from the center O, and the most distant point P_{max} is at a distance $(R + r)$ from the center, then, by (7), the radial velocity of P_{min} at time t is $H(t)(R - r)$, wile that of P_{max} is $H(t)(R + r)$

After a small time t_1, P_{min} reaches the position: P'_{min} so that

$$P'_{min}P_{min} = \int_{t_0}^{t_0+t_1} H(s)(R - r)ds \qquad (10)$$

And P_{max} reaches the position: P'_{max} so that

$$P_{max}P'_{max} = \int_{t_0}^{t_0+t_1} H(s)(R + r)ds \qquad (11)$$

Then the new diameter $P'_{min}P'_{max}$, can be expressed with respect to $r = P_{min}P_{max}$ via:

$$P'_{max}P'_{min} = P'_{max}P_{max} + P_{max}P_{min} - P_{min}P'_{min}$$

$$= \int_{t_0}^{t_0+t_1} H(s)(R + r)ds + 2r - \int_{t_0}^{t_0+t_1} H(s)(R - r)ds = 2r\left(1 + \int_{t_0}^{t_0+t_1} H(s)ds\right)$$

$$P'_{min}P'_{max}, = 2r\left(1 + \frac{2}{3}[lns]_{t_0}^{t_0+t_1}\right) = 2r\left(1 + \frac{2}{3}ln\frac{t_0 + t_1}{t_0}\right) \qquad (12)$$

After t_1 time, the diameter 2r in the line of sight (aligned with the central origin O) will be stretched by the amount

$$\left(1 + \frac{2}{3}ln\frac{t_0 + t_1}{t_0}\right), \qquad (13)$$

that depends on the elapsed time t_1 and the age t_0 of U, when the disc was placed (born) inside U.

Since we know, the rotational velocity is given by [Kallel-Jallouli, 2024a]:

$$V_{rot}(R) = \frac{2\pi R}{T} = \frac{2\pi R}{\sqrt{kR^3}} = \frac{2\pi}{\sqrt{kR}}, \qquad (14)$$

then, the diameter 2r, perpendicular to the line of sight (from the central origin O) remains unchanged. So, by relation (13), more the elapsed time t_1 is higher, more our circle will be elongated in the line of sight (from the origin O), and the eccentricity of our seen "deformed ellipse" will be higher. Consequently, if we place a small subhalo U' inside a big halo U, far from the center O of U, we have to expect the circular Keplerian orbits inside U' to become elongated (deformed elliptical trajectories). The elongation is bigger for higher periods (see relation (13)) and then for farther objects from the U' center. The elongation will be at its maximum (maximum eccentricity) when the plane of the orbit is aligned with O, and the period is high. An orbit perpendicular to the line of sight from O remains circular.

Our seen universe U' is a subuniverse of a bigger huge tectonic Old-iceball U called Feluc, as proposed by Kallel in her new Big Bang theory [Kallel-Jallouli S, 2018, 2024b]. We can then explain the strongly flattened

ISSN No. 2321-2705 | DOI: 10.51244/IJRSI |Volume XI Issue XI November 2024

high-redshift galaxies [Ceverino et al., 2015], confirmed by NASA's James Webb Space Telescope (JWST) [Pandya et al. 2024] (fig.1) and the absence of any flattened or elongated shapes near our galaxy.

Fig. 1 A distant galaxy identified in Webb's CEERS Survey (NIRCam Image) [https://webbtelescope.org/contents/news-releases/2024/news-2024-104#section-id-2]

Discontinuity of the trajectories Phase shift.

We are always interested in an isolated halo U. Let 's consider a test particle P in a Keplerian circular orbit in the equatorial plane around the origin, with a period T_1. If at the universal time t_U=t_0, P is placed (born) at a distance R_1 from the origin, with an initial phase $\theta_{1,0}$, then, at each instant $t < T_1$, while P advances in its orbit around the origin, its distance $R_1(t)$ from the origin will be stretched (13), via:

$$R_1(t) = R_1\left(1 + \frac{2}{3} ln \frac{t_U + t}{t_U}\right) \quad (15).$$

After one revolution (T_1 time), P will tend to be at a farther distance R_2 from the origin, satisfying:

$$R_2 = R_1\left(1 + \frac{2}{3} ln \frac{t_0 + T_1}{t_0}\right) \qquad (16).$$

Remarks

1. For the special case when we suppose the period T_1 equals the age t_0 of U, when P (was born and) begun its revolution:

$$T_1 = t_0, \qquad (17)$$

Then, we get:

$$R_2 = R_1\left(1 + \frac{2}{3} ln2\right) \qquad (18)$$

Reciprocally, if we suppose we have the relation (18), then, the period T_1 is given by (17).

2. If the universe U contains a massive spinning particle P in Keplerian orbits, then, since the particle is receding from the halo center, then, P get farther from the halo center. The day become longer (time delay) [Kallel-Jallouli, 2024a], leading to an apparent decrease in the rotational speed of the particle, as measured by fixed clocks. If we do not care about the change in the physical "Zaman time", there will appear to be no conservation of angular momentum!

ISSN No. 2321-2705 | DOI: 10.51244/IJRSI |Volume XI Issue XI November 2024

For $0 < t < T_1$, the phase θ satisfies using (5):

$$\frac{\theta}{2\pi} = Int\left[\frac{t+t_0}{T_1}+1\right] - \frac{t+t_0}{T_1} \qquad (19)$$

At $t = 0$, the beginning phase $\theta_{1,0}$ satisfies, using (5):

$$\frac{\theta_{1,0}}{2\pi} = Int\left[\frac{t_0}{T_1}+1\right] - \frac{t_0}{T_1} \qquad (20)$$

When P tends to complete its first revolution, the quantity $\frac{\theta}{2\pi}$ tends to

$$\frac{\theta_{1,f}}{2\pi} = Int\left[\frac{T_1+t_0}{T_1}+1\right] - \frac{T_1+t_0}{T_1} = Int\left[\frac{t_0}{T_1}+1\right] - \frac{t_0}{T_1} = \frac{\theta_{1,0}}{2\pi} \qquad (21)$$

And the phase tends to $\theta_{1,0}$. The particle tend to complete one full revolution, with an open orbit.

Unfortunately, the second revolution will have a new period $T_2 > T_1$, since the starting new radius $R_{2,0}$ satisfies (16):

$$R_{2,0} = R_1\left(1+\frac{2}{3}ln\frac{t_0+T_1}{t_0}\right) > R_1 \quad (22)$$

and using the relation (6), we have:

$$\frac{{T_2}^2}{{R_{2,0}}^3} = \frac{{T_1}^2}{{R_1}^3} \qquad (23)$$

By replacing $R_{2,0}$ using (22) inside (23), we get:

$$T_2 = T_1\left(1+\frac{2}{3}ln\frac{t_0+T_1}{t_0}\right)^{3/2} > T_1 \quad (24)$$

P will restart its second revolution at the new universal time $T_1 + t_0$. Unfortunately, the new starting phase $\theta_{2,0}$ must satisfy the law (5) of its relation to the period:

$$\frac{\theta_{2,0}}{2\pi} = Int\left[\frac{T_1+t_0}{T_2}\right] + 1 - \frac{T_1+t_0}{T_2} \neq \frac{\theta_{1,f}}{2\pi} = \ Int\left[\frac{t_0}{T_1}+1\right] - \frac{t_0}{T_1} \qquad (25)$$

This means that; at the universal time $T_1 + t_0$, P will receive a kick-off to change its phase position instantaneously; instead of starting its novel trajectory from the final phase $\theta_{1,f} = \theta_{1,0}$, P will jump to restart generally at a different phase $\theta_{2,0} \neq \theta_{1,0}$, with a starting radius $R_{2,0}$ given by (22).

Moreover, since the function f defined for $x > 0$, by $f(x) = Int[x] - x$, is strictly increasing for $x\epsilon]0,1[$, and strictly decreasing for $x > 1$, then, for $T_2 < T_1 + t_0$, we get $\theta_{2,0} > \theta_{1,f}$, and P will shift to an advanced phase, instantaneously.

For the second revolution, the starting new universal time is $t_U = t_0 + T_1$. For $0 < t < T_2$, the radius $R_{2,0}$ will be stretched. Using (15)(22), we can write:

$$R_2(t) = R_{2,0}\left(1+\frac{2}{3}ln\frac{t_0+T_1+t}{t_0+T_1}\right) = R_1\left(1+\frac{2}{3}ln\frac{t_0+T_1}{t_0}\right)\left(1+\frac{2}{3}ln\frac{t_0+T_1+t}{t_0+T_1}\right) \quad (26)$$

ISSN No. 2321-2705 | DOI: 10.51244/IJRSI |Volume XI Issue XI November 2024

P will continue its third revolution, at the new universal time $t_U = t_0 + T_1 + T_2$, with a new orbital period $T_3 > T_2$, and a new starting phase $\theta_{3,0}$, shifted from the previous starting phase $\theta_{2,0}$. For $0 < t < T_3$, the distance $R_3(t)$ is given by (using (15)):

$$R_3(t) = R_{3,0}\left(1 + \frac{2}{3} ln \frac{t_0 + T_1 + T_2 + t}{t_0 + T_1 + T_2}\right) \qquad (27)$$

with

$$R_{3,0} = R_{2,0}\left(1 + \frac{2}{3} ln \frac{t_0 + T_1 + T_2}{t_0 + T_1}\right) \qquad (28)$$

At its n[th] revolution ($n > 2$), the departure of P will start, at the universal time $t_U = t_0 + \sum_{i=1}^{n-1} T_i$, from the starting phase $\theta_{n,0}$ shifted from the previous one $\theta_{n-1,0}$. Moreover, the new period T_n is greater than the previous one T_{n-1}. The new period T_n satisfies the recurrent relation:

$${T_n}^2 = {T_{n-1}}^2\left(1 + \frac{2}{3} ln \frac{t_0 + T_1 + \cdots + T_{n-1}}{t_0 + T_1 + \cdots + T_{n-2}}\right)^3 \qquad (29)$$

The starting phase $\theta_{n,0}$ satisfies:

$$\frac{\theta_{n,0}}{2\pi} = Int\left[\frac{t_0 + T_0 + \cdots + T_{n-1}}{T_n}\right] + 1 - \frac{t_0 + T_0 + \cdots + T_{n-1}}{T_n} \qquad (30)$$

For $0 < t < T_n$, P will be at a distance :

$$R_n(t) = R_{n,0}\left(1 + \frac{2}{3} ln \frac{t_0 + T_0 + \cdots + T_{n-1} + t}{t_0 + T_0 + \cdots + T_{n-1}}\right) \qquad (31)$$

The starting distance $R_{n,0}$ at the universal time $t_0 + \sum_{i=1}^{n-1} T_i$ is given by the recurrent relation:

$$R_{n,0} = R_{n-1,0}\left(1 + \frac{2}{3} ln \frac{t_0 + \sum_{i=0}^{n-1} T_i}{t_0 + \sum_{i=0}^{n-2} T_i}\right) \qquad (32)$$

Evidently, this spontaneous phase shift, after each revolution, must be accompanied with spontaneous energy exchange. The spontaneous energy release is known in the case of electrons inside an atom. In the case of astronomical haloes, matter ejection was detected to propagate out of the orbital plane of a compact object. A kick can accelerate the rotation of a star by transferring angular momentum to its crust.

The n[th] scale factor "a_n"

If at the universal time $t_U = t_0$, a test particle P is placed (or born) at a distance R_1 (with period T_1 satisfying relation (6)) from the origin, with phase position $\theta_{1,0}$, then, after t' time, the particle will be at a distance $R(t')$ from the origin, that can be written in the form:

$$R(t') = R_1 a_n(t_0, T_1, t') \qquad (33)$$

With, for the first period, $n = 1$, $t' = t < T_1$ (see relation (15)),

$$a_1(t_0, T_1, t) = \left(1 + \frac{2}{3} ln \frac{t_0 + t}{t_0}\right) = a_1(t_0, t) \qquad (34)$$

We call the factor $a_1(t_0, t)$ the "first scale factor". It depends on the universal time t_0, and the time t. For any particle P placed (or born) at a distance R_1, the "first scale factor" satisfies:

ISSN No. 2321-2705 | DOI: 10.51244/IJRSI |Volume XI Issue XI November 2024

$$1 \le a_1(t_0,t) \le a_1(t_0,T_1) \qquad (35)$$

If we differentiate the first scale factor with respect to time, we obtain the known relation:

$$\frac{da_1(t_0,t)}{dt} = \frac{2}{3}\frac{1}{t_0+t} = H(t_U)\,, \qquad for \quad t < T_1 \qquad (36)$$

The second derivative:

$$\frac{d^2a_1(t_0,t)}{dt^2} = -\frac{2}{3}\frac{1}{(t_0+t)^2} = -\frac{3}{2}H(t_U)^2, \quad for \quad t < T_1 \qquad (37)$$

The deceleration parameter q_0 given by:

$$q_0 = -\frac{a_1''}{a_1 a_1'^2} > 0, \qquad (38)$$

is clearly positive.

For the second period, $n = 2$, as we can deduce from (26), if $T_1 < t' = T_1 + t < T_1 + T_2$, then:

$$a_2(t_0,T_1,t') = a_1(t_0,T_1)\left(1 + \frac{2}{3}ln\frac{t_0+T_1+t}{t_0+T_1}\right) = a_1(t_0,T_1)a_1(t_0+T_1,t) \qquad (39)$$

The second scale factor $a_2(t_0,T_1,t')$ depends on the universal time t_0, when the particle P was at a distance R_1 from the central origin. Moreover, it also depends on R_1 (position of P)(or equivalently on T_1) , and then on the redshift z_1 ($z_1 = \frac{H}{c}.R_1$, see [Kallel-Jallouli, 2024a]). For any particle P placed (or born) at a distance R_1, the "second scale factor" satisfies:

$$a_1(t_0,T_1) \le a_2(t_0,T_1,T_1+t) \le a_1(t_0,T_1)a_1(t_0+T_1,T_2) \qquad (40)$$

Differentiating (39) with respect to time, we get for $T_1 < t' = T_1 + t < T_1 + T_2$:

$$\frac{da_2(t_0,T_1,t')}{dt} = \frac{2}{3}a_1(t_0,T_1)\frac{1}{t_0+T_0+t} = a_1(t_0,T_1)H(t_U) \qquad (41)$$

For the nth period ($n > 2$), if $\sum_{i=1}^{n-1}T_i \le t' = t + \sum_{i=1}^{n-1}T_i < \sum_{i=1}^{n}T_i$, then,

$$a_n(t_0,T_1,t') = a_1(t_0+T_1+\cdots+T_{n-1},t)a_1(t_0,T_1)\prod_{i=1}^{n-2}a_1(t_0+T_1+\cdots+T_i,T_{i+1}) \qquad (42)$$

This nth scale factor a_n depends on the universal time t_0, when the particle P was at a distance R_1 from the central origin. Moreover, it also depends on the beginning place of each orbit $(R_j)_{j\le n-1}$ (or equivalently on T_j) , then on the redshifts $(z_j)_{j\le n-1}$ ($z_j = \frac{H(t_0+\sum_{i=1}^{j-1}T_i)}{c}.R_j$, see [Kallel-Jallouli, 2024a]). For any particle P placed (or born) at a distance R_1, the "nth scale factor" satisfies:

$$a_1(t_0,T_1)\prod_{i=1}^{n-2}a_1(t_0+T_1+\cdots+T_i,T_{i+1}) \le a_n\left(t_0,T_1,\sum_{i=1}^{n-1}T_i+t\right) \le a_1(t_0,T_1)\prod_{i=1}^{n-1}a_1(t_0+T_1+\cdots+T_i,T_{i+1}) \qquad (43)$$

ISSN No. 2321-2705 | DOI: 10.51244/IJRSI |Volume XI Issue XI November 2024

As we can deduce from (42), the derivative of the n[th] scale factor $a_n(t_0, T_1, t')$ is given by:

$$a'_n(t_0, T_1, t') = C_n(t_0, T_1)H(t_0 + T_0 + \cdots + T_{n-1} + t) = C_n(t_0, T_1)H(t_U) \quad (44)$$

With $C_n(t_0, T_1)$ is a constant satisfying the recurrence relation:

$$C_{n+1}(t_0, T_1) = C_n(t_0, T_1)\left(1 + \frac{2}{3} ln \frac{t_0 + T_1 + \cdots + T_n}{t_0 + T_1 + \cdots + T_{n-1}}\right), \ n > 2 \quad (45)$$

With

$$C_2(t_0, T_1) = \left(1 + \frac{2}{3} ln \frac{t_0 + T_1}{t_0}\right) \quad (46)$$

We can see from (44)(45)(46), the derivative of the n[th] scale factor, $a'_n(t_0, T_1, t')$, is equal to the Hubble constant, only for the case n=1 (only for one cycle of a particle). Otherwise, we get a constant $C_n(t_0, T_1)$ multiplied by the Hubble constant.

To get a good approximation to the Hubble constant in the relation (44), $C_n(t_0, T_1)$ must be close to 1, or equivalently, the time t' must be negligible compared to t_0 , i.e. : $t' \ll t_0$.

In practice, for example, in the case of our solar system U_S, we can determine, experimentally, for each planet P, the starting position R_1(P), and the final position $R_2(P)$ after one complete revolution. Then, since k is known, we can deduce the period T_1 from the relation (6). Then, using the relation (33), we can calculate the first scale factor $a_1(t_0, T_1)$ via

$$\frac{R_2}{R_1} = a_1(t_0, T_1) = \left(1 + \frac{2}{3} ln \frac{t_0 + T_1}{t_0}\right) \quad (47)$$

We can then, from relation (47), deduce the age t_0 of the solar system U_S, when P started its orbit at a distance R_1 from the sun, via the relation

$$t_0 = \frac{T_1}{e^{\frac{3}{2}\left(\frac{R_2}{R_1} - 1\right)} - 1} \quad (48)$$

Since $R_2(P)$ is known, we can deduce the period T_2, from the relation (6).

We can also deduce the phase shift $\theta_{2,0}$ after one orbit via (25).

So, the knowledge of the beginning distance R_1 from the central origin, and the final distance R_2, after one complete revolution, is sufficient to deduce : T_1 and T_2 via the Kepler relation (6), the age t_0 of the system U when the test particle was at R_1, via the relation (48), then the first scale factor $a_1(T_1, t)$ via the relation (32). We can also deduce the phase shift $\theta_{2,0}$ via the relation (25). The age t_0 of the system U can also be deduced via the formula (25), if the phase shift $\theta_{2,0}$ can be experimentally measured. Some corrections must be taken into consideration since our solar system is not lodged inside an isolated halo.

Some strange astronomical phenomena

Matter ejection from a star in orbit inside a microquasar

Microquasars are binary star systems consisting of a normal star and a compact object, typically a black hole or a neutron star. The material from the normal star is accreted onto the compact object, forming an accretion gaseous disk around it, called an accretion disk.

ISSN No. 2321-2705 | DOI: 10.51244/IJRSI |Volume XI Issue XI November 2024

A complex process, within the accretion disk and between the disk and the compact object, can lead to the emission of intense X-rays and the ejection of material in the form of relativistic jets perpendicular to the plane of the disk at all times. In general, the disc is precessing along with the jets around the same axis and at the same angular frequency. The exact mechanism triggering these ejections and the timescales involved were not yet fully understood.

LS I +61◦303

LS I +61 303 constitutes a high-mass X-ray binary system, part of our own galaxy, the Milky Way. It is situated in the constellation Cassiopeia, which is visible from Earth. LS I +61°303 was located at a distance of 2.0 ± 0.2 kpc [Frail & Hjellming, 1991], but now, it is located at a distance of 2.65 ± 0.09 kpc [Weng et al., 2022]. LS I +61 303 is comprising a compact companion of uncertain identity, potentially a neutron star, more likely a pulsar according to Weng et al. (2022), or conceivably a black hole as suggested by Casares et al. (2005). The compact companion orbits a massive, early-type B0 Ve donor star, characterized by rapid rotation, on an eccentric orbit (e = 0.72 ± 0.15, as reported by Casares et al., 2005), while undergoing mass loss via a high-velocity stable equatorial disk, commonly referred to as an accretion disc [Casares et al. 2005]. The orbital period of the binary system, P = 26.4960 ± 0.0028 d [Gregory 2002], is slightly higher than the previous one 26.4917± 0.0025 [Gregory et al. 1999]. An increasing period by about 3 s per year for SS433 microquasar was identified [Cherepashchuk et al., 2021]

During the orbital motion, the compact object in LS I +61◦303, accreting material from the Be donor, undergoes a periodical (P1~26.49 days) ejection of relativistic outflow of material, at a particular orbital phase around periastron, forming two precessing (P2~26.9±0.1 d) conical jets.

The ejected cloud expands linearly along the direction of the rotation axis of the accretion disc, perpendicular to the accretion disk plane [Massi & Torricelli-Ciamponi, 2014] [Hjellming & Johnston 1988][Martí & Paredes 1995], giving rise to the expanding double radio source observed with radio interferometers [Massi, 1993]. Only one outburst per orbit was observed [Gregory, 2002][Abdo et al. 2009]**.** Synchrotron emission from relativistic particles refilling the jets, produces a maximum when the jet electron density is at its maximum [Massi et al. 2015].

The star is encompassed by a disc of accreting material, which rotates at a nearly Keplerian velocity [Chernyakova 2023]. The Keplerian velocity gradually decreases with distance from the star, reaching its minimum at the truncation radius of the disc. The rotation period at the disc truncation radius is [Chernyakova 2023]

The plasma clouds are ejected during the replenishment of the inner part of the accretion disk [Greiner et al. 1996], that follows its sudden disappearance beyond the last stable orbit around the compact companion (probably black hole). Only some fraction is propelled into synchrotron-emitting clouds of plasma .The collision of relativistic ejecta with environmental material has been observed in real time [Hjellming et al. 1998], where the leading edge of the jet decelerates while strongly brightening [Mirabel and Rodríguez,1999]. The size of the jet can be much greater than the orbital size. A tail length of about 6.5mas was detected [Dhawan et al. 2006]. Emitting regions are perpendicular to the jet. The γ-ray emitting region is assumed closer to the compact object than the observed radio jets [Kniffen et al. 1997]. There is a time lag between the start time of the ejection near periastron and the onset of the observed radio-outburst. In the case of LSI+61°303 the radio outbursts occurs about 10 days after the periastron passage. More generally, the onset of the outburst should be observed earlier at higher frequencies [Taylor & Gregory 1982]. The higher frequencies tend to peak earlier and fade more quickly than the lower frequencies. A mean time delay between the 8.3 GHz outburst and the 2.25 GHz outburst of 0.4 days was measured. There is an apparent lengthening of the measured period between outbursts for lower frequencies [Ray et al. 1997][Paredes et al. 1997].

The radio emission appears cometary, with a ‘tail’ pointing away from the high-mass star. the cometary head traces an erratic ellipse, of semi-major axis that can be about 4 times the binary axis [Dhawan et al. 2006].

The ejecta in quasars and microquasars move with relativistic speeds [Mirabel & Rodríguez 1999]. But in

ISSN No. 2321-2705 | DOI: 10.51244/IJRSI |Volume XI Issue XI November 2024

microquasars (the black hole is only a few solar masses) the particles ejected at relativistic speeds, from the black hole, can travel up to distances of a few light years only, instead of several million light years as in giant radio galaxies (multiple million solar masses black hole) [Mirabel & Rodríguez, 1998].

What mechanism may cause the disappearance of the inner accretion disk and the sudden matter ejection?

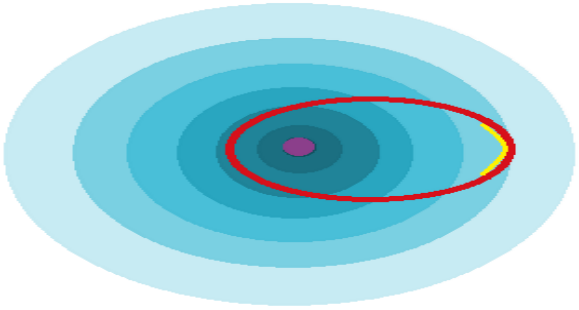

Figure 2: Orbit of the compact object travelling through the halo of the Be star. Radio outbursts in LS I +61◦303 occur around apastron passage (in yellow). However, near periastron gamma-ray emission is observed (but no radio emission). The yellow curve is inspired from [Massi 2004].

Around periastron, a high-energy outburst was detected, but radio emission was absent [Abdo et al. 2009]

Why no radio bursts are observed at periastron passage? Why does the radio bursts occur only around apastron passage (fig. 2)?

The morphology varies dramatically near periastron, with outflow velocities ∼7500 km/s, and dimunishes gradually around the rest of the orbit, to be $\sim 1000\ \mathrm{km/s}$ near apastron [Dhawan et al. 2006]. A rotation of the inner structure and rapid changes in the orientation of the cometary tail at periastron were detected [Dhawan et al. 2006].

The emission peak intensity positions trace the place downstream in the tail**.** The peak intensity image is further displaced radially outward from the pulsar orbit, for longer wavelengths, and lags by days in time, compared to shorter wavelengths [Dhawan et al. 2006, figure 4].. Comparing 13 cm and 3.6 cm images, we can deduce the existence of synchrotron opacity gradient along the cometary tail, pointing away from the high-mass star, with the highest-energy particles located in the head [Dhawan et al. 2006].

GRS 1915+105

The microquasar GRS 1915+105 is a binary system, located in the galactic plane inside our Galaxy, in the constellation Aquila, at a distance of ∼11–12 kpc [Mirabel & Rodríguez 1994][Fender et al. 1999]. The normal star is a K iii companion with a 0.8 ± 0.5 $M_\odot$ [Greiner et al, 2001]. The compact object in GRS 1915+105, is a black hole (BH) with a mass $M_{BH} = 12.4^{+2}_{-1.8}\, M_\odot$ [Reid et al. 2014], orbiting the center of mass of the system with a period of 33.5 ± 1.5 d [Greiner et al, 2001].

The apparent position of the BH core position in the binary system GRS 1915+105 reveals some "jitter" along the jet axis at certain times [Reid et al. 2014], that can be related to the orbital motion. This jitter could be associated with the production of low-level jet emission [Reid et al. 2014], indicating that the processes driving the jets can influence the apparent BH core position. Despite the orbital motion, the predicted positional jitter due to the black hole's orbit around the binary system's center of mass is very small, approximately 0.004 milliarcseconds (mas) [Reid et al. 2014].

At regular intervals, the accretion disk, which surrounds the BH in GRS 1915+105, disrupts and throws off its inner portion. The abrupt vanishing of the inner accretion disk, detected in the X-rays, triggers the formation of relativistic expanding clouds of plasma observed at longer wavelengths [Mirabel et al. 1998] [Mirabel & Rodríguez 1999]. This disk of matter re-forms itself after each powerful jet, as the black hole pulls in more matter from its companion star. The black hole, in the constellation Aquila, throws off, periodically, the mass

ISSN No. 2321-2705 | DOI: 10.51244/IJRSI |Volume XI Issue XI November 2024

equal to that of a 100 trillion ton asteroid at nearly the speed of light approximately 650 million miles per hour. This process clearly requires a lot of energy, each cycle. The jet material must come from the inner disk [Greiner et al., 1996].

If we examine the source on a longer timescale, larger superluminal jets appear at the same trigger point, just much less often than the smaller ones. After the flare, we can see slower replenishment of the inner region of the accretion disk. From 1994 January-August data, the time separation between ejections for GRS 1915+105 suggests a quasi-periodicity at intervals in the range of 20-30 days [Rodriguez & Mirabel, 1999]. The kinetic energy of the plasma clouds suggests an unclear acceleration mechanism with very large power [Rodriguez et al. 1995]. The inner disk region empties and refills on timescales of seconds. The jets of GRS 1915+105 carry an important amount of energy away from the central source into the interstellar medium.

Pulsar glitches

It's widely accepted in astrophysics that radio pulsars are rapidly rotating highly magnetized neutron stars formed as a result of supernova explosions from their progenitor stars. They initially have rapid rotation speeds, around 50 Hz, shortly after their formation. However, within a few hundred thousand years, they slow down to longer periods due to the braking torque exerted by their high magnetic field strengths ($\sim 10^{12}$ G) [Bailes et al. 2011]. As pulsars rotate, they emit electromagnetic radiations in form of cones out of their magnetic poles tilted with respect to their rotation axes. As these beams sweep across space as the star rotates, much like the beam of a lighthouse, they create pulses of radiation that can be observed when they cross the observer's line of sight. Once their rotation periods reduce to a few seconds, the majority of pulsars cease emitting radio waves [Bailes et al. 2011].

Pulsars rotation rates can be remarkably stable over long periods. They are used to be the most stable 'clocks' in the universe. Even as these pulses remain unbelievably regular, pulsars gradually lose their rotational kinetic energy, leading to a smooth decrease in their spin rate over time, as rotational energy transforms into an electromagnetic outflow [Helfand et al. 2001].

In general, pulsar's slow-down is smooth and continuous. However, the rotation of young pulsars, such as the Crab pulsar (B0531+21), is occasionally disturbed by discrete spin-up incidents known as glitches. Pulsar glitches are typically characterized by sudden rapid rises in rotation rate or spin frequency ($\Delta\nu$) [Espinoza et al. 2011][Yu et al. 2013]. This discontinuous increase of the spin-frequency of a pulsar, or fractional decline in rotation period (ΔP) is followed by a gradual return to the pre-glitch rotation rate over time.

PSR B2035+36

The pulsar PSR B2035+36 (J2037+3621) is an isolated relatively old radio pulsar discovered in 1985 [Dewey et al. 1985], with 0.6187 s period and -4.5024×10^{-15} s s^{-1} period derivative [Hobbs et al. 2004].

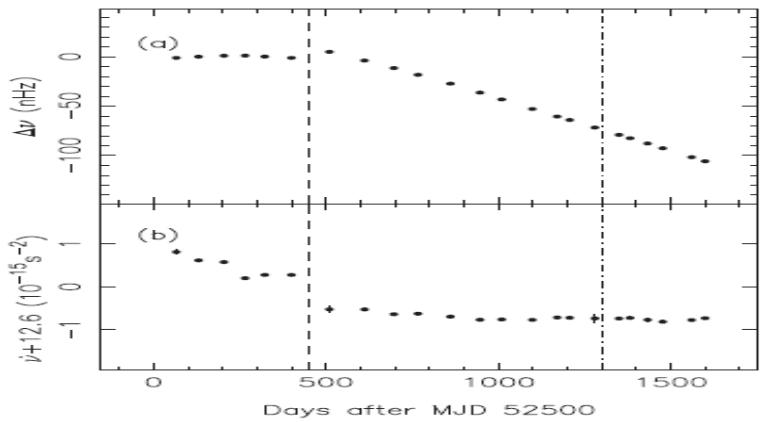

Figure 3. [Kou et al. 2018, fig.1) Variations of ν and ˙ν of PSR B2035+36. (a) Variations of frequency ν relative to the pre-glitch solutions; (b) variations of the first frequency derivatives. The dashed line is the glitch epoch of MJD 52950.

ISSN No. 2321-2705 | DOI: 10.51244/IJRSI |Volume XI Issue XI November 2024

Around MJD 52950, PSR B2035+36 experienced a glitch (fig.3), characterized by a frequency jump of approximately $\Delta\nu \sim 12.4(5)$ nHz [Kou et al. 2018]. The observed large glitches were attributed to a sudden angular momentum transfer deposited into the solid crust causing it to spin-up [Zhao et al. 2017]. A sudden apparent change in a neutron star's moment of inertia has been detected during a glitch event [Zhao et al. 2017].

PSR B0833-45

Glitches can potentially affect the position of a pulsar, although the effect would be very small and difficult to detect directly. The sky coordinates of the Vela pulsar PSR B0833-45 centroid exhibited sinusoidal wanderings [Helfand et al. 2001].

The two polar jets, seen in the Vela pulsar PSR B0833-45, must be supplied with particles from the pulsar [Helfand et al. 2001]. The energy input from a glitch must be deposited at the base of the crust within the star, the response of the star's magnetosphere could result in the release of energy to diffuse outward [Helfand et al. 2001] [Kou et al. 2018]. The pulsar spin-down rate, after-glitch, implies an energy loss. What causes a glitch to occur?

Spruit & Phinney suggested that the rotation axes and space velocities of pulsars could be connected through the nature of the "kicks" given to neutron stars [Spruit & Phinney, 1998].

PSR B0919+06

The pulsar PSR B0919+06 , also known as PSR J0923+08, estimated to be located at a distance of about 1,200 light-years from Earth, is part of a binary system, its companion likely being a white dwarf star [Gong et al. 2018]. The orbital period of this binary system, which is the time it takes for the pulsar and its companion to complete one orbit around their common center of mass, is measured to be around 10 minutes.

PSR B0919+06 is characterized by its relatively strong radio emissions, featuring a rotational frequency of $\nu = 2.3$ Hz and a deceleration rate of $\dot{\nu} = -7.4 \times 10^{-14}$ Hz s^{-1} [Manchester et al. 1978].

An unusual spinning up, with an amplitude of approximately 10 milliseconds occurring over roughly 10-minute intervals (specifically 14 minutes), was initially detected in the singular pulsar PSR B0919+06 [Rankin et al. 2006]. The spin-up can be related to the presence of an orbiting celestial body [Wahl et al. 2016] [Gong et al. 2018].

A kick can accelerate the rotation of a star by transferring angular momentum to it. When we refer to a "kick" in the context of stellar dynamics, we typically mean a sudden increase in momentum, often caused by asymmetric supernova explosions or gravitational interactions in binary systems. This asymmetric ejection can cause the remnant core, such as a neutron star or a black hole, to receive a kick, leading to an increase in its rotational velocity about its own axis rather than its orbital motion around another object. If a kick accelerates the rotation of a star, it primarily affects the star's rotation rate and do not necessarily cause the orbital motion of surrounding objects to accelerate.

Break-up velocity

The break-up angular velocity (the maximum velocity at which it can rotate) of a star, with mass M, radius R, core rotation Ω, can be calculated by equating centrifugal acceleration with gravity:

$$\Omega^2 r_* = GM_*/r_*^2 \qquad (49)$$

Most stars in fact rotate well below the break-up rotation rate given by:

$$\Omega_{\mathrm{br}} \sim \sqrt{GM/R^3} \qquad (50)$$

Which clearly decreases as the star's radius R increases.

ISSN No. 2321-2705 | DOI: 10.51244/IJRSI |Volume XI Issue XI November 2024

At the rotating star surface, mass loss happens when the surface rotation rate Ω_s reaches the break-up limit Ω_{br}, above which the star will be forced to centrifugally expel mass. Basically, this mass outflow arises from the fact that matter is rotating at a lower rate than the star.

In binary systems where the main star has accreted in its disk enough mass from a companion donor star, the small amounts of accreted matter can be enough to replenish the angular momentum of the main star, causing it to increase the its surface rotation rate towards the break-up limit [Ryan et al. 2002], triggering centrifugal mass loss, from their equatorial regions [Hartmann & MacGregor, 1982], and increasing the X-ray luminosity [Bhattacharyya & Chakrabarty, 2017]. A part of the accreted matter (the inner disk) is thrown away from the system by two bipolar outflows [Hartmann & MacGregor 1982]. This ejected matter takes away angular momentum from the main star [Tauris 2012]. Ejected matters are loaded with disc material but their power is borrowed from the stellar rotational energy reservoir [Hartmann & MacGregor 1982]. The ejected mass carries away enough angular momentum and slows down the rotation rate of the star to prevent the star from ever rotating near breakup.

When the accretion disk is emptied by the enhanced accretion rate, the source returns to an extended X-ray quiescent state. A new outburst occurs when sufficient mass accumulates in the disk again [Done et al. 2007].

Accretion from a binary companion can be crucial for supplying enough angular momentum to drive centrifugal mass loss [Bhattacharyya & Chakrabarty, 2017]. jets from discs can only carry away the exact fraction of disc angular momentum, leading to a spin-down, and allowing matter to be accreted by the star [Bhattacharyya & Chakrabarty, 2017].

DISCUSSIONS AND CONCLUSIONS

In the previous work [Kallel-Jallouli, 2024a], the author studied the case of an isolated Zaman Dark Matter halo U with differential rotation; where each shell of radius R rotates with a period T(R), related to R via the Kepler relation: $\frac{T^2(R)}{R^3} = k$, for $R > r_0$. Let us call this halo U: an "outer Keplerian universe" (OKU). Kallel proved that the Hubble's law (7)(8) is valid inside any OKU, without any need for any supplementary hypothesis or any non-Euclidean geometry on U [Kallel-Jallouli, 2024a]. She has just used her proposed Zaman DM model [Kallel-Jallouli, 2021a,b,c,d]. Moreover, let's consider the more general case when the period T of each shell of radius R is related to R via [Kallel-Jallouli, 2024a]

$$\mathrm{T} = f(\mathrm{R}), \qquad (51)$$

with f is a one-to-one positive function. Then, if f is a decreasing function, any test particle inside U, satisfying relation (51) feels a gravitational attraction to the Halo center (Dark Matter effect). If f is an increasing function, any test particle inside U, satisfying relation (48) feels a gravitational expulsion from the Halo center (Dark energy effect). Therefore, Zaman spin gradient results in the appearance of Dark Matter and Dark Energy.

In this present study, we proved the Keplerian trajectories inside an OKU do not fully overlap. Moreover, after each period, any test particle P inside U receives a kick-off and instantaneously shifts to a phase position higher than the previous one, to continue its next cycle. The phase shift is a well known phenomenon. For Mercury, advance of the perihelion is measured to be about 9.55 arc minutes per century. This measured phase shift can be deduced by only knowing the distance R_1 from Mercury to the sun and the age t_0 of the solar system U_S at the time of measurement. We can then, deduce the period T_1 via the Kepler formula (6), then the distance $R_{2,0}$ after one period via (22). The new period T_2 can be calculated via (23). We can deduce the phase shift $\theta_{2,0}$ via the relation (25).

We can also use the knowledge of the distance between the moon and our earth to deduce the age of our earth-moon system U_E. It is not difficult to measure the distances R_1 and R_2. It is not difficult to measure the periods T_1 and T_2. Equation (48) allows to deduce the age t_E of the system U_E when the moon was at the distance R_1 from earth. We can also deduce the phase shift $\theta_{2,0}$ of the moon after each orbit, via the relation

ISSN No. 2321-2705 | DOI: 10.51244/IJRSI |Volume XI Issue XI November 2024

(25). Evidently, since U_E is not an isolated halo (it is a subhalo of the solar system halo U_S), some corrections must be added to the theoretical solutions.

The scale factor $a_n(t_0, T_1, t')$ depends on the universal time t_0, when the particle P was placed (or boen) at a distance R_1 (related to T_1 via the Kepler relation (6)) from U-center. When we differentiate the scale factor with respect to time, we find the Hubble constant only for an elapsed time $t' < T_1$. Otherwise we get the Hubble constant multiplied by a constant $C_n(t_0, T_1)$, that can be close to 1 only if the time t' is negligible with respect to the age t_0 of U.

Since after each complete cycle, a particle P in its Keplerian orbit is instantaneously shifted, this will give a tremendous energy to the kicked particle. It will spin up and we can explain most of the strange astronomical phenomena given in paragraph 8. The spin up of the star crust will cause it to rotate much higher than the surrounding magnetosphere and inner accretion disk. The crust length of the day will be smaller than the surrounding inner accretion disk length of the day. The created high gravity (by Zamn spin gradient) will be directed outward as Kallel explained [Kallel-Jallouli, 2024a], and the nearest inner part will be ejected outward.

Now, we shall explain the absence of radio wavelengths when the associated star is nearer to the center, in its trajectory inside a binary system.

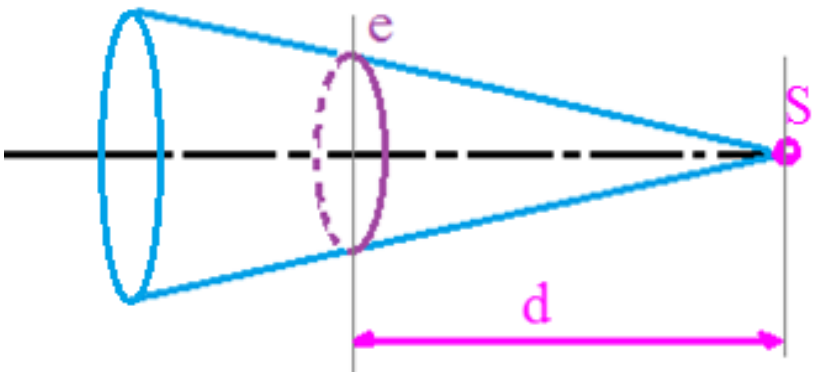

Fig.4. The jet emission region e that produces Gamma rays at periastron, at a distance d from the accretor star center S.

Suppose the gamma photons are ejected at periastron, from a source e at a distance d to the accretor star S (fig.4). Since the distance between the two stars is at the minimum a (fig. 2), the distance between e and the central star will be $a_1 = a + d$. When the accretor star will at apastron, at a distance b> a from the centeral star (fig. 2), the distance between e and the central star will be $b_1 = b + d > a_1$ (The jet is always directed outward). Suppose the detector is aligned with the apastron-peristron position, in the peristron direction. When passing from the distance a_1, where the radial velocity v_1 is subjected to the relation [Kallel-Jallouli, 2024a] :$v_{1r} = H_1\, a_1$,and the circular velocity is given by [Kallel-Jallouli, 2024a]: $v_{1c} = \frac{2\pi}{{a_1}^{1/2}}$, to the distance b_1 where the radial velocity v_2 satisfies the relation :$v_{2r} = H_1\, b_1$, and the circular velocity is given by: $v_{2c} = \frac{2\pi}{{b_1}^{1/2}}$, neglecting the effect of circular velocity, then the observed frequency from periastron passage is given by [Kallel-Jallouli, 2024a]:

$$\nu_{p.obs} = \left(1 - \frac{V_r.\hat{r}}{c}\right)\nu_e = \left(1 + \frac{v_{1r}}{c}\right)\nu_e \qquad (52)$$

And the observed frequency from apastron passage is given by

$$\nu_{a.obs} = \left(1 - \frac{v_{2r}}{c}\right)\nu_e \qquad (53)$$

The difference between the two frequencies when passing from peristron to apastron is given by:

ISSN No. 2321-2705 | DOI: 10.51244/IJRSI |Volume XI Issue XI November 2024

$$\Delta\nu = \nu_{p.obs} - \nu_{a.obs} = \left(\frac{v_{1r} + v_{2r}}{c}\right)\nu_e = \frac{H_1}{c}(a_1 + a_2)\nu_e \quad (54)$$

This relation means that, when the star passes from peristron to apastron, the light emitted from point e will be redshifted. Reciprocally, when the star passes from apastron to peristron position, the received light will be blueshifted. This explains why in some binary systems, we detect gamma rays at periastron passage, but we detect longer waves (radio waves) at apastron passage, from the same emitter source.

Moreover, from relation (54), if we know the emitted and observed light frequencies, and the distances a_1 and a_2, then, we can calculate H_1, and then deduce the age of the binary system.

More calculations will be explicitly given in future works, to deduce experimentally the age of an OKU system and the phase shift of a particle in Keplerian motion inside it.

REFERENCES

1. A. Abdo, M. Ackermann, M. Ajello, et al. (2009). Fermi LAT observations of LS I+ 61 303: first detection of an orbital modulation in GeV gamma rays. The Astrophysical Journal, 701(2), L123
2. M. Bailes et al. (2011), Transformation of a star into a planet in a millisecond pulsar binary, Science, 333(6050), 1717-1720.
3. S. Bhattacharyya, & D. Chakrabarty, (2017). The effect of transient accretion on the spin-up of millisecond pulsars. The Astrophysical Journal, 835(1), 4
4. J. Casares, I. Ribas, J. M. Paredes, J. Martí, C. Allende Prieto, (2005). Orbital parameters of the microquasar LS I+ 61 303. Monthly Notices of the Royal Astronomical Society, 360(3), 1105-1109
5. D. Ceverino, J. Primack & A. Dekel, (2015), Formation of elongated galaxies with low masses at high redshift, Monthly Notices of the Royal Astronomical Society, Volume 453, Issue 1, 11 October, Pages 408–413,
6. M. Chernyakova, (2023). Energy-dependent periodicities of LS I +61◦303 in the GeV band, MNRAS 525, 2202–2207
7. M. Cherepashchuk, A. A. Belinski, A. V. Dodin, K. A. Postnov, (2021). "Discovery of orbital eccentricity and evidence for orbital period increase of SS433". Monthly Notices of the Royal Astronomical Society: Letters. 507 (1): L19–L23.
8. T. Clifton, P. G. Ferreira, A. Padilla, & C. Skordis, (2012). Modified gravity and cosmology. Physics reports, 513(1-3), 1-189
9. R. J. Dewey, J. H. Taylor, J. M. Weisberg, G. H. Stokes, (1985), A search for low-luminosity pulsars. Astrophysical Journal, Part 2-Letters to the Editor (ISSN 0004-637X), vol. 294, p. L25-L29. NSF-supported research.
10. V. Dhawan, A. Mioduszewski, & M. Rupen, (2006), LS I +61◦303 is a Be-Pulsar binary, not a Microquasar, Proceedings of the VI Microquasar Workshop, 52.1, Como, Italy
11. R. H. Dicke, P. J. E. Peebles, P. G. Roll, & D. T. Wilkinson, 1965, ApJ, 142, 414
12. Done, M. Gierliński, & A. Kubota, (2007). Modelling the behaviour of accretion flows in X-ray binaries: Everything you always wanted to know about accretion but were afraid to ask. The Astronomy and Astrophysics Review, 15, 1-66.
13. M. Espinoza, A. G. Lyne, B. W. Stappers, & M. Kramer, (2011), A study of 315 glitches in the rotation of 102 pulsars. Monthly Notices of the Royal Astronomical Society, 414(2), 1679-1704
14. A. Frail & R. M. Hjellming, (1991), Distance and total column density to the periodic radio star LSI+ 61 deg 303. Astronomical Journal (ISSN 0004-6256), vol. 101, p. 2126-2130.
15. B. P. Gong, Y. P. Li, J. P. Yuan et al. (2018), "Searching Ultra-compact Pulsar Binaries with Abnormal Timing Behavior." The Astrophysical Journal 855.(1) 35.
16. P. C. Gregory, (2002), Bayesian analysis of radio observations of the Be X-ray binary LS I +61_303, ApJ, 575, 427
17. P. C. Gregory, M. Peracaula, & A. R. Taylor, (1999), Bayesian periodic signal detection II. Discovery of periodic phase modulation in LS I +61º303 radio outbursts. ApJ, 520, 376-390
18. J. Greiner, J. G. Cuby & M. J. McCaughrean, (2001). An unusually massive stellar black hole in the Galaxy. Nature, 414(6863), 522-525

19. J. Greiner, E. Morgan, and R. A. Remillard, (1996), Rossi x-ray timing explorer observations of GRS 1915+ 105. The Astrophysical Journal, 473(2), L107
20. L. M. K. B. Hartmann, & K. B. MacGregor, (1982). Protostellar mass and angular momentum loss. Astrophysical Journal, Part 1, vol. 259, p. 180-192.
21. J. Helfand, E. V. Gotthelf & J. P. Halpern, (2001). Vela pulsar and its synchrotron nebula. The Astrophysical Journal, 556(1), 380-391
22. R. M. Hjellming & K. J. Johnston, 1988, Radio emission from conical jets associated with X-ray binaries. Astrophysical Journal, Part 1 (ISSN 0004-637X), vol. 328, p. 600-609.
23. R. M. Hjellming, M. P. Rupen, A. M. Mioduszewski et al. (1998), in Workshop on Relativistic Jet Sources in the Galaxy. Paris, December 12-13, 1998
24. Hobbs et al., (2004), The Parkes multibeam pulsar survey–IV. Discovery of 180 pulsars and parameters for 281 previously known pulsars. Monthly Notices of the Royal Astronomical Society, 352(4), 1439-1472
25. S. Kallel-Jallouli, (2018), Discover the big bang and the secrets of our universe. A new theory. CreateSpace Independent Publishing Platform, ISBN-13: 978-1719246859
26. S. Kallel-Jallouli, (2021a), The mystery of time I. A new model to solve the enigma of Dark Matter, Internationl Kindle, Independent Publishing Platform, ISBN-13: 979-8514538751
27. S. Kallel-Jallouli, (2021b), The mystery of time: A New Solution for Dark Matter and a Better Understanding of Quantum Mechanics. J Pur Appl Math, 5(4): 32-37
28. S. Kallel-Jallouli, (2021c), A New Solution for Dark Matter and a Better Understanding of Quantum Mechanics. J. Phys. Math. Vol.12, N. 8
29. S. Kallel-Jallouli, (2021d). A new Geometrical Model to solve the Puzzle of Time and understand the mystery of Dark Matter and the magic of Quantum Mechanics., 5th Conference on Mathematical Science and Applications, KAUST, DOI: 10.13140/RG.2.2.22841.95843
30. S. Kallel-Jallouli, (2023), Time Dark Matter geometrical model and Newton's law recovery, International Journal of Research and Innovation in Applied Science. Vo. IX, issue III, p. 406-410.
31. S. Kallel-Jallouli, (2024a), Keplerian motion inside an isolated Dark Matter halo, International Journal of Research and Scientific Innovation, 11(9), 1225-1235
32. S. Kallel-Jallouli, (2024b), The Big Bang explosion and the creation of our universe. “Time” Zero. DOI: 10.13140/RG.2.2.14477.72167
33. S. Kallel-Jallouli, (2024c), A new geometrical time model to explain the discrepancy between theoretical and measured velocities, Research Gate DOI: 10.13140/RG.2.2.18508.39048
34. S. Kallel-Jallouli, (2024d), No more twin paradox, International Journal of Research and Innovation in Applied Science. Vo. IX, issue III, p. 77-88.
35. D. A. Kniffen, W. C. K. Alberts, D. L. Bertsch, et al. (1997), Egret observations of the gamma-ray source 2CG 135+01. ApJ, 486, 126
36. F. Kou, J. P. Yuan, N. Wang, W. M. Yan and S. J. Dang, (2018). The spin-down state change and mode change associated with glitch activity of PSR B2035+36, MNRAS 478, L24–L28
37. E. J. Lerner, R, Falomo, and R. Scarpa, (2014). UV surface brightness of galaxies from the local universe to z ~ 5, International Journal of Modern Physics D Vol. 23, No. 6, 1450058 (21 pages)
38. F. Mirabel and L. F. Rodríguez, (1999), Sources of relativistic jets in the galaxy, https://arxiv.org/pdf/astro-ph/9902062.pdf
39. R.P. Fender, S.T. Garrington, D.J. McKay et al. (1999). MERLIN observations of relativistic ejections from GRS 1915+105. Mon. Not. R. Astron. Soc. 304, 865-876
40. M. Massi, (2004). Introduction to Astrophysics of Microquasars, “Habilitation” University of Bonn
41. M. Massi, F. Jaron, & T. Hovatta, (2015), Long-term OVRO monitoring of LS I +61◦303: confirmation of the two close periodicities, A&A, 575, L9
42. Martí, & J.M. Paredes, (1995), Modelling of LSI+ 61 303 from near infrared data. Astronomy and Astrophysics, v. 298, p. 151,
43. M. Massi, J. M. Paredes, R. Estalella, & M. Felli, (1993), High resolution radio map of the X- ray binary LS1+61º303 A&A, 269, 249
44. M. Massi & G. Torricelli-Ciamponi, (2014), Intrinsic physical properties and Doppler boosting effects in LS I +61◦303, A&A 564, A23
45. F. Mirabel, V. Dhawan, S. Chaty et al. (1998), Accretion instabilities and jet formation in GRS 1915+

ISSN No. 2321-2705 | DOI: 10.51244/IJRSI |Volume XI Issue XI November 2024

105. Astronomy and Astrophysics, v. 330, p. L9-L12
46. F. Mirabel, L.F. Rodríguez (1994). A Superluminal Source in the Galaxy. Nat. 371, 46-48.
47. V. Pandya, H. Zhang, M. Huertas-Company et al. (2024), Galaxies Going Bananas: Inferring the 3D Geometry of High-Redshift Galaxies with JWST-CEERS, to appear in ApJ
48. M. Paredes, J. Marti, M. Peracaula, & M. Ribo, (1997). Evidence of X-ray periodicity in LSI+ 61 303. Astronomy and Astrophysics, 320, L25-L28.
49. Planck Collaboration XIII. 2016, Cosmological parameters, A&A, 594, A13
50. Planck Collaboration VI. Cosmological parameters, 2020, A&A, 641, A6
51. Perivolaropoulos, 2014, Large Scale Cosmological Anomalies and Inhomogeneous Dark Energy, Galaxies, 2, 22-61
52. Petrovic, N. Langer, & K. A. van der Hucht, (2005), Constraining the mass transfer in massive binaries through progenitor evolution models of Wolf-Rayet+ O binaries. Astronomy & Astrophysics, 435 (3), 1013-1030
53. J. M. Rankin, C. Rodriguez, & G. A. Wright, (2006). Bistable profile illumination in pulsars B0919+ 06 and B1859+ 07. Monthly Notices of the Royal Astronomical Society, 370 (2), 673-680.
54. P. S. Ray , R. S. Foster , E. B. Waltman et al. (1997). Long-Term Flux Monitoring of LSI +61◦ 303 at 2.25 and 8.3 GHz. The Astrophysical Journal, 491, 381-387, 1997
55. J. Reid, J. E. McClintock, J. F. Steiner et al. (2014), A parallax distance to the microquasar GRS 1915+ 105 and a revised estimate of its black hole mass, ApJ, 796 (1), 2
56. G. Riess, L. M. Macri, S. L. Hoffmann, et al. (2016). A 2.4% determination of the local value of the Hubble constant. The Astrophysical Journal, 826(1), 56.
57. G. Riess, L. Macri, S. Casertano, et al. (2011). A 3% solution: determination of the Hubble constant with the Hubble Space Telescope and Wide Field Camera 3. The Astrophysical Journal, 730(2), 119
58. F. Rodriguez, & I. F. Mirabel, (1999). Repeated relativistic ejections in GRS 1915+ 105. The Astrophysical Journal, 511(1), 398.
59. F. Rodriguez, E. Gerard, I. F. Mirabel, Y. Gómez, & A. Velázquez, (1995). Radio monitoring of GRS 1915+ 105. Astrophysical Journal Supplement, 101, 173.
60. S. G. Ryan, S. G. Gregory, U. Kolb, T. C. Beers, & T. Kajino, (2002). Rapid rotation of ultra-Li-depleted halo stars and their association with blue stragglers. The Astrophysical Journal, 571(1), 501.
61. H. Spruit, & E. S. Phinney, (1998). Birth kicks as the origin of pulsar rotation. Nature, 393(6681), 139-141.
62. T. M. Tauris, (2012). Spin-down of radio millisecond pulsars at genesis. Science, 335(6068), 561-563.
63. R. Taylor & P. C. Gregory, (1982), PERIODIC RADIO EMISSION FROM LS I +61°303, Astrophys. J. 255, 210-216
64. H. M. Wahl, D. J. Orfeo, J. M. Rankin and J. M. Weisberg. (2016). Quasi-Periodicities in the Anomalous Emission Events in Pulsars B1859+07 and B0919+06. MNRAS 461, 3740–3746
65. S. S. Weng, L. Qian, B. J. Wang, et al. (2022). Radio pulsations from a neutron star within the gamma-ray binary LS I +61° 303. Nat Astron 6, 698–702
66. Yu, R. N. Manchester, G. Hobbs, et al. (2013). Detection of 107 glitches in 36 southern pulsars. Monthly Notices of the Royal Astronomical Society, 429(1), 688-724
67. J. Zhao et al., (2017), Mode change of a gamma-ray pulsar, PSR J2021+ 4026, ApJ, 842 (1), 53